كلية الهندسة بشبرا
FACULTY OF ENGINEERING AT SHOUBRA
ERJ
PRINT ISSN 3009-6049
ONLINE ISSN 3009-6022

ENGINEERING RESEARCH JOURNAL (ERJ)
Volume (53) Issue (2)
April 2024, pp:10-25
https://erjsh.journals.ekb.eg

Flexural Strength of Cold Formed Section with Laterally Restrained Tension Flange

Anwar Badawy Abu-Sena[1], Maged Tawfick Hanna[2], Maro Nashaat Helal[*1], Khaled A. M. Gharib[1]

[1] Department of Civil Engineering, Faculty of Engineering at Shoubra, Benha University, Cairo, Egypt
2Housing and Building National Research center (HBRC), Egypt.
[*] Corresponding Author.
E-mail: abbadawy@yahoo.com, magedtawfick@gmail.com, kh_am50@yahoo.com Maro.nashaat@hotmail.com

Abstract: This research reports a numerical study on the flexural strength of single-lipped Zed-Purlin sections under two equal moments applied at the ends of the specimen. The effects of attaching corrugated steel sheeting to the tension flange of Z-purlins on the structural behavior are investigated. The studied parameters of the specimens are: types of corrugated steel sheeting, depth-to-thickness ratio, and the span of the purlins. Linear and non-linear analyses using finite element software are conducted. Results show that a tension flange braced by corrugated steel sheeting can increase the section capacity of Z-purlins and change the failure mode. The results of the ultimate moment obtained from finite element analysis have been compared to both the nominal flexural strength according to the Egyptian code (ECP) and the North American Specifications (AISI). The results of purlins with sheeting determined by ECP are conservative due to ignoring the effect of corrugated steel sheeting on capacity, while the results from AISI are in good agreement with finite element analysis as they take into account the effect of sheeting.

Keywords: purlins, Z sections, flexural strength, tension flange, lateral support.

1. INTRODUCTION

Cold-formed sections are popularly used in structural applications, e.g., roof trusses, mainframe members, purlins, and girts, due to their high strength-to-weight ratio, flexibility to produce any shape suitable to the requirements of a particular application, and economics [1, 2]. However, these sections are weak in torsional stiffness, and their large width to thickness ratio can cause them to fail into three different modes: local, distortional, and overall buckling [3–4]. There are several cross sections of cold formed steel such as C, Z, ∑ and Π. The roof panel provides full lateral and partial torsional bracing for the top flange of Z-section-purlins. The roof panel is simulated by two components: lateral and rotational springs, as suggested by Ye et al. [5].

Li, L. Y. [6] studied analytical models to determine the lateral torsional buckling of Z-purlin laterally restrained by sheeting subject to different cases of loading (pure bending, uniformly distributed gravity and uplift loading) with different boundary conditions. An experimental and numerical studies are carried out to determine the section capacity of Z-purlin when the tension flange is restrained to a standing seam roof by fasteners, with and without a tie rod subject to uplift loading by (Luan, W., & Li, Y. Q.[7]). The energy method is utilized to determine the effect of lateral bracing provided by sheeting on the lateral torsional buckling of a Z-purlin beam with different parameters (boundary conditions, location of load, tie rods), Chu et al. [8]. GAO, T., & Moen, C. D [9] determined the flexural response of simple purlins subject to outward wind loading using the direct strength method. Balazs et al. [10] investigate experimentally the influence of sandwich panels on the capacity of Z-purlin under outward wind loading.

Li et al. [11] investigated experimentally the influence of shear fasteners on structural behavior of cold formed section. Ren et al. [12, 13, and 14] studied the flexural strength of both Z-section and C-section attached to roof panels, which was represented as a lateral support act at the line of web-flange junction and rotation spring stiffness acts at the middle of the flange.

In their studies, the purlin is simply supported and subjected to uniform load upward.

Zhang et al. [15] studied the structural behavior of channel purlins roof system under uplift uniform load. In-addition, they considered thickness of both the purlin and sheeting, types of profile sheeting, location and number of tie rods. The author reported that the tie rod could affect the capacity and change the failure modes. Huang, R., & Luan, W. [16] studied the structural behavior of Z-purlin when tension flanges were restrained by sheeting under uplift loading. Their results are compared to different codes (Chinese code (GB50018), Euro-code (EC3), and other codes that take into account the restraint provided by sheeting in calculations.

Yu, C., & Yan, W. [17] reported an effective width method for evaluating the distortional buckling of both C and Z-sections. Wibbenmeyer [18] investigated experimentally purlin roof system consisting of Z-purlin with depth 305mm connected with roof panels by self-drilling screws subjected to outward wind loading. He recommended the reduction factor to be 0.598.

Almatrafi et al. [19, 20] studied experimentally and numerically the structural behavior of a two Z-sections with lips placed in the opposite direction subjected to four points of downward loading linked to cladding sheeting by fasteners in the presence of angle struts. Moreover, the influence of the length of the lip in the Z section on the flexural strength was considered.

The Egyptian code [21] did not take into account the effect of restraint provided by sheeting for uplift loading compared with the AISI code [22]. Therefore, the present research aims to study the flexural resistance of a lipped Z-section purlin under two equal moments applied at the end of the specimen. Finite element analysis model is generated and validated with experimental works conducted by Almatrafi et al., [19]. Then, the parametric numerical study is presented to study the influence of corrugated steel sheeting connected to the tension flange on the moment resistance of the Z-section. Finally, the results of finite element analysis are compared to the AISI 2020 design specifications and the ECP 2008.

2.Finite Element Analysis

2.1 Finite element modelling

The finite element program ABAQUS [23] is used to perform elastic linear buckling analysis in order to obtain Eigen value and buckling mode shapes. Then the critical buckling shape was scaled by imperfection value, to be considered as the initial imperfect shape of the non-linear analysis conducted. The S4R shell element, that is a linear 4-nodded shell element with reduced integration was used to model both purlins and sheeting. A thin, flexible in shear, isometric quadrilateral shell element is the one that is used. The element size utilized in the finite element mesh is 12mm as recommended by Almatrafi et al., [20], in order to gain sufficiently accurate findings from the finite element analysis.. The Young's modulus is considered 210 GPa, and the Poison ratio is 0.3. The considered nominal yield strengths are 345 MPa and 245 MPa for purlins and sheeting profiles, respectively. Figure (1) shows the finite element model used in this study.

A perfect plasticity model is utilized to simulate the stress-strain curve.

In order to simulate the interaction between the purlin and sheeting, a general contact is assumed: hard behavior in the normal direction and frictionless behavior in the tangential direction. The considered initial imperfection value is L/1000 for global buckling mode, where L is the length of purlin. While for local or distortional buckling mode, the value is taken as 0.1t, where t is the thickness of the purlin.

The self-drilling screws are applied in the form of tie constraints to connect purlin and sheeting at different points, which are applied at 200 mm. All section nodes at the end of the member were coupled to a point at the mid-height of the web, where loads and boundary conditions are applied. The loads are applied in the form of moments about the major axis to create tension at the lower flange (restrained flange) while the upper flange (free flange) is under compression. This case occurs in practice when purlins are subjected to uplift wind loads. The boundary conditions at the end sections are such that the horizontal lateral movement (U_x) and the vertical movement (U_y) are restrained, while the rotation about the longitudinal axis (UR_z) is prevented along the line of the web only. Also, at the mid-span section, the longitudinal movement (U_z) is restrained at all nodes.

The boundary conditions of sheeting are as follows: horizontal lateral movement in the X-direction (Ux), rotation about the longitudinal axis (URz), and rotation about the vertical axis (UR_y) are prevented. Figure 2 shows the boundary conditions for both purlin and sheeting.

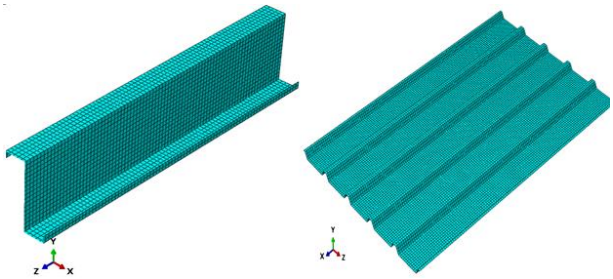

a)Purlin’s mesh b) Sheeting mesh

Fig 1. Purlin and sheeting mesh sizes

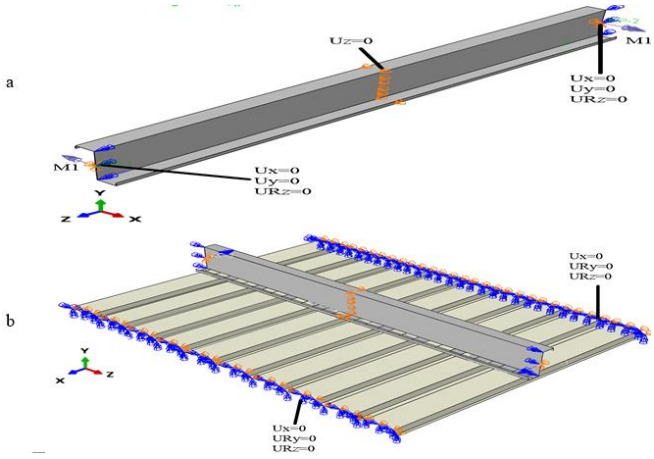

Fig 2. boundary conditions a) for purlin, b) for sheeting

2.2 Finite element validation

Verification of the finite element model has been made by comparing its results with Almatrafi et al. [19] work. The imperfection values are combined between the local buckling value of 0.1t or 0.54 t and the distortional buckling value of 1.14 t. A true stress-strain curve is used, similar to that in Almatrafi et al. [20]. Due to symmetry, only half of the model is conducted. Two models are considered. In the first (Model 1), a single Z-section purlin was connected with both sheeting and angle struts. (Model 2) consists of a single Z-section purlin connected with sheeting, while the angle struts was represented by lateral support. The Z-section has a 3000mm span, while the cladding sheeting has a width of 250 mm, linked by self-drilling screws at every 400mm. In addition, angle struts have a width of 250 mm. They are placed at the mid-depth of the web at a spacing of 600 mm. The specimens are subjected to four points of loading downward at the web-flange junction. The cladding is applied on the compression side.

TABLE 1. Purlin cross sections Almatrafi et al. [19] and figure 3 cross section

Section	h (mm)	b (mm)	d mm)	t (mm)	r mm)
Z14613	145.41	61.37	18.61	1.28	4.31
Z14620	145.68	63.35	17.34	1.96	4.07
Z17613	176.75	61.71	19.51	1.29	3.84
Z17625	176.13	63.7	20.95	2.47	4.05
Z20620	200	66.4	19.64	1.95	4.44
Z24615	239.75	65.3	20.47	1.48	3.8
Z24620	243.83	66.35	19.5	2	4
Z30718	300.25	75.1	16.95	1.76	4.05

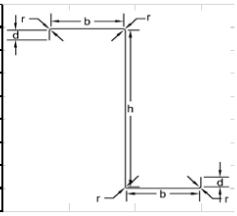

The types of elements and mesh sizes for both Z-section and cladding are the same as described in Section 2.1. The mesh size of angle struts is 5 mm by 5 mm. Points are created on the compression flange to connect to sheeting with self-drilling screws. The boundary conditions are the same as in Section 2.1, with the exception of two components: longitudinal movement (U_z) is restrained at the center of the web applied at the end of the purlin, and vertical rotation (UR_y) and longitudinal rotation (UR_z) are restrained at the center of the web at both ends. (See Figure 4). The material properties of steel are as follows: Young's modulus is 200 GPa, the poison ratio is 0.3, and the maximum tensile nominal strength is 585.91 MPa according to the true stress-strain curve. Eight specimens are validated using finite element models. Table 1 shows the cross-section details, where h is the height of the purlin, b is the width of the flange, d is the lip depth, r is the radius of intersection between web and flange, and t is the thickness of the purlin.

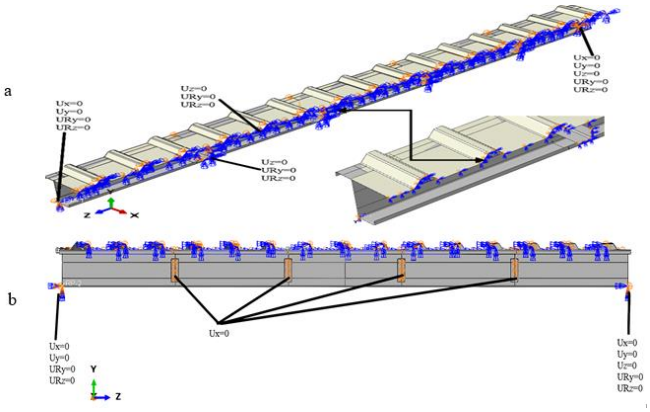

Fig 4. Boundary conditions of purlin, sheeting and angle struts: a) for (Model 1) and b) for (Model 2) according to reference [20]

Figure 5 shows a vertical displacement response for sections Z14613 and Z14620, which agrees well with the experimental work at the peak point. Table 2 shows the ultimate moment value for both the experimental work (M_T) and the finite element analysis ultimate moments M_{u1} and M_{u2} of (Model 1) and (Model 2) respectively. The values of the specimens show good agreement with each other. In the first (Model1), the difference in ultimate moment between numerical and experiment data is not more than 2.4% except for the section of Z14613, which is 6.5%, and the average value is 1.01. In the second (Model2), the difference in ultimate moment between numerical and experiment data does not exceed 2.6%, except in section Z14613, where it is 6% and the average ratio is 1.008. Figure 6 shows the deformed shape of sections Z14620 and Z17625 under four points of loading, which agree well with the experiment results.

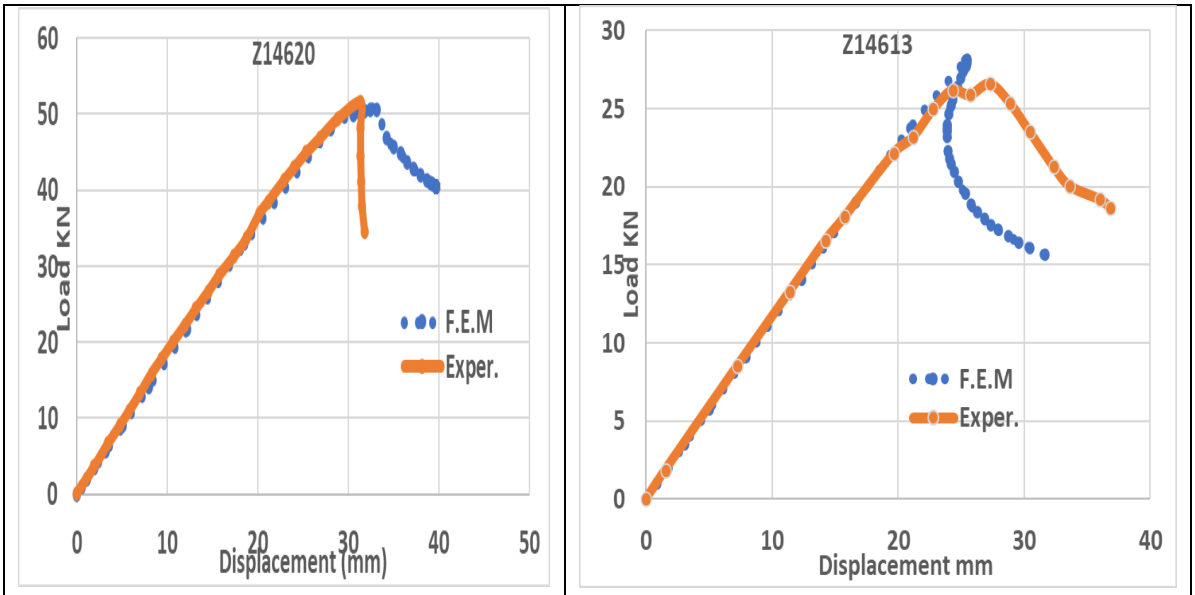

a) section Z14620 b) section Z14613

Fig 5. vertical-displacement response for section Z14620 and Z14613

TABLE2. Results of ultimate moment and failure modes of experimental results [19] and numerical calculations.

Section	Exper.	Model 1			Model 2			Failure mode	
	M_T (kN.m)	M_{u1} (kN.m)	M_{u1}/M_T	Error (%)	M_{u2} (kN.m)	M_{u2}/M_T	Error (%)	Exp.	Finite Element
Z14613	5.94	6.33	1.065	6.5	6.3	1.06	6	D/L interaction	D/L interaction
Z14620	11.54	11.39	0.987	-1.3	11.25	0.974	-2.6	D	D
Z17613	7.03	7.18	1.021	2.1	7.11	1.021	2.1	D/L	D/L
Z17625	19.77	19.98	1.011	1.06	19.81	1.002	0.2	Yield followed by D/L interaction	Yield followed by D/L interaction
Z20620	15.62	15.61	0.999	0	15.57	0.997	-0.3	D followed by WC	D followed by WC
Z24615	11.55	11.83	1.024	2.4	11.64	1.008	0.8	D/L	D/L
Z24620	20.33	20.22	0.994	-0.6	20.19	0.994	-0.6	D	D
Z30718	19.13	19.48	1.018	1.8	19.35	1.012	1.2	D followed by WC	D followed by WC

D: Distortional buckling, L: local buckling, WC: web crippling

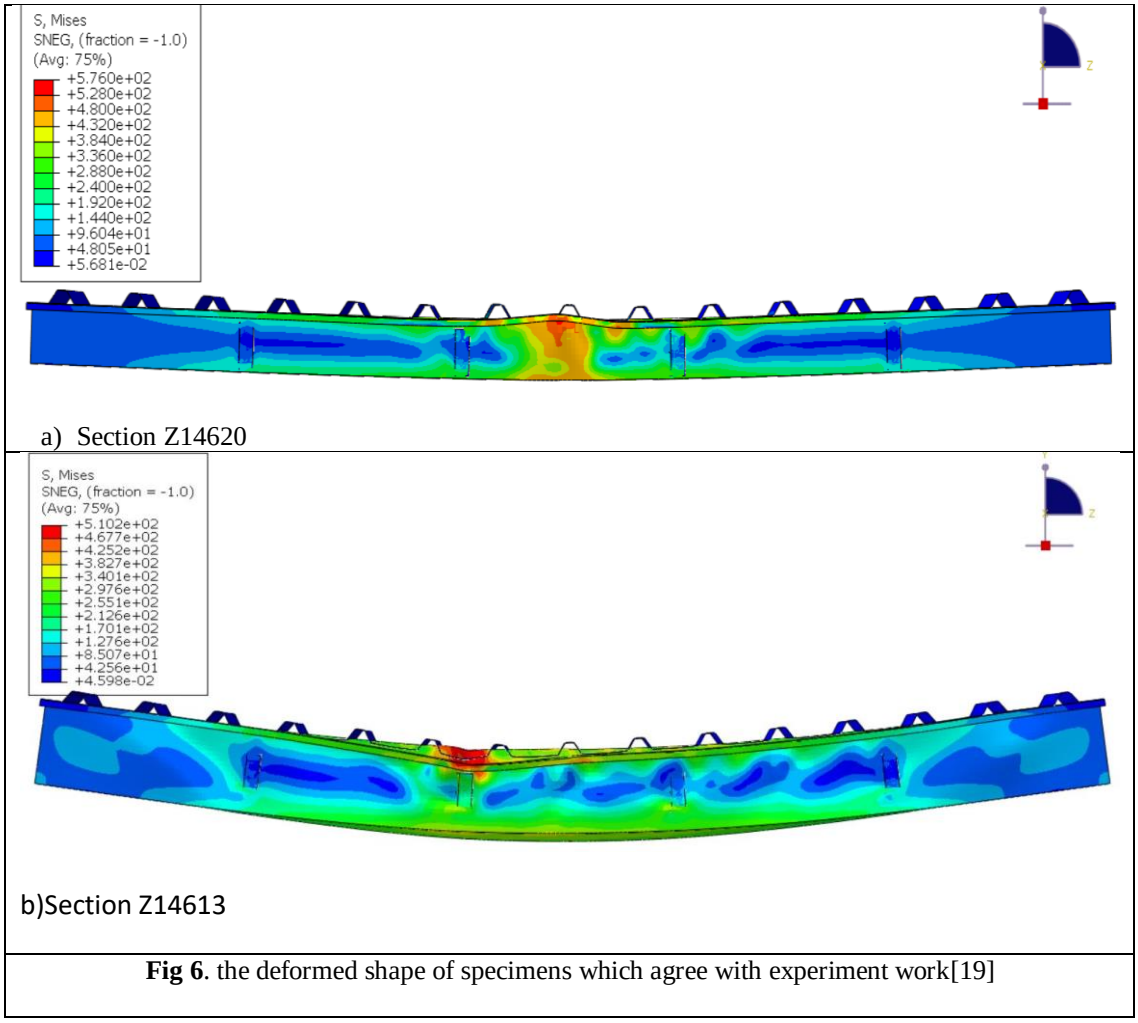

Fig 6. the deformed shape of specimens which agree with experiment work[19]

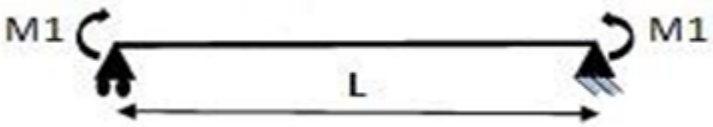

Fig 7. Purlin subject to two equal end moment

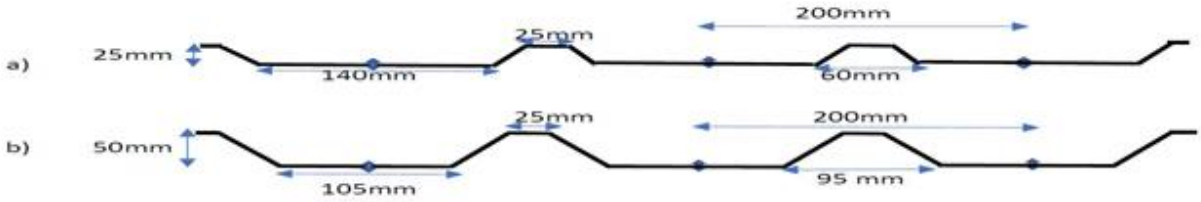

Fig 8. Roof profile corrugated sheeting. a) Profile No. 1 (P1), b) Profile No. 2 (P2)

TABLE 3. Dimension of Z- purlin studied

Section	h mm	b mm	d mm	t mm
Z175*1.5	175	62.5	20	1.5
Z175*2	175	62.5	20	2
Z175*2.5	175	62.5	20	2.5
Z200*1.5	200	65	20	1.5
Z200*2	200	65	20	2
Z200*2.5	200	65	20	2.5
Z265*1.5	265	65	20	1.5
Z265*2	265	65	20	2
Z265*2.5	265	65	20	2.5

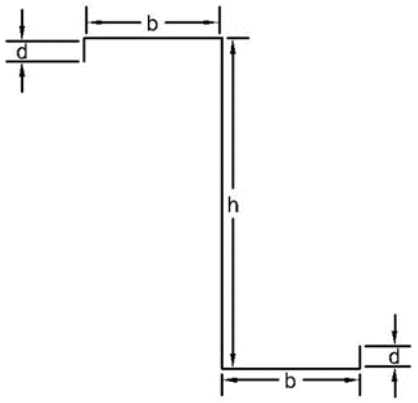

TABLE4. The R-factor for Z-purlin

Depth of purlin (mm)	R factor
d≤165mm	0.7
165<d≤216mm	0.65
216<d≤305mm	0.5

3. Parametric Study:

In this study specimens are divided into two groups. First group represents purlins without sheeting, while in the second group sheeting is modeled to consider its effect. First group consists of single lip Z-section purlin that is subject to two equal end moments. Second group, consists of corrugated steel sheeting attached to the tension flange of a Z section-purlin by self-drilling screws subject to two equal end moments (see Figure7). All purlins are pin-ended. The lengths of purlins are 2000mm, 4000mm, 6000mm, 8000mm, and 10000mm. The width of corrugated steel sheeting that represents the spacing between purlins is 1500mm. The specimens are modelled for both linear and non-linear analysis.

Nine specimens of different cross-sections of the lipped Z-section are selected from Albion Sections [24]. Table3 shows the dimensions of Z-purlin.

Two types of roof profiles with a thickness of 0.5 mm are chosen, namely profile No. 1 (P1) and second profile No. 2 (P2) (see figure 8), where roofs P1 and P2 are YX25-200 and YX50-200, respectively, according to Zhang et al. [15]. Profile No.1 has a height of 25 mm, and profile No.2 has a height of 50mm. The spacing between self-drilling screws is taken 200 mm.

Beams will be refereed to Zh*t-L-Q, Where Zh*t refers to the cross section of purlin as h is the height of the web, t is the thickness of the purlin.L is the length of the specimen and Q refers to the types of corrugated steel sheeting as profile No.1 (P1) and profile No.2 (P2). For example, Z175*1.5- 6-P1, where Z175*1.5 is the section, the length of the specimen is 6000 mm and P1 refers to sheeting profile (No. 1).

4. Nominal Strength in Design Codes

The nominal strengths are evaluated according to the Egyptian code [21] and AISI-2020 [22]. A brief review of codes provisions for estimating nominal strength of Z purlins has been provided hereafter.

4.1. AISI-2020 Code:

The nominal strength is estimated using the following equations for purlins without and purlins with sheeting when the tension flange is restrained and the free flange is under compression:

The moment resistance of Z-purlin with sheeting (M_n) is determine depending on the effective width method from equation (1):

$$M_n = R\, M_{n/o} \quad (1)$$

R: the reduction factor depends mainly on the depth of web (see table 4)

$M_{n/o}$: Nominal flexural strength with consideration of local buckling only

The nominal flexural strength for Beams for Z-purlin without sheeting is determined by the Direct Strength Method (DSM). It is defined as the minimum of three values (Mnl, Mnd, and Mne) evaluated using equation (2).

$$\frac{M_{ne}}{M_y} = \frac{10}{9}\left(1 - \frac{10M_y}{36M_{cre}}\right)$$
$$\frac{M_{nl}}{M_{ne}} = \left(1 - 0.15\left(\frac{M_{crl}}{M_{ne}}\right)^{0.4}\right)\left(\frac{M_{crl}}{M_{ne}}\right)^{0.4}$$
$$\frac{M_{nd}}{M_y} = \left(1 - 0.22\left(\frac{M_{crd}}{M_y}\right)^{0.5}\right)\left(\frac{M_{crd}}{M_y}\right)^{0.5} \quad (2)$$

M_{cre}: Critical elastic lateral torsional buckling moment.
M_{ne}: Nominal flexural strength for lateral torsional buckling.
M_{crl}: Critical elastic local buckling moment.
M_{nl}: Nominal flexural strength for local buckling.
M_{crd}: Critical elastic distortional buckling moment.
M_{nd}: Nominal flexural strength for distortional buckling

4.2. Egyptian code of practice (ECP):

According to the ECP [21], the moment resistance is determined according to the effective width method for purlins. ECP does not consider the sheeting that is attached to the tension flange of the purlin. The moment resistance value (M_n) is determined from the smallest of the following equations:

a) $M_n = F_L S_{eff.}$ (3)

S_{eff}: effective section modulus about major axis
$F_L = 0.6 F_y$

b) $M_n = C_b M_{cr}$ (4)

C_b: Bending coefficient depending on moment gradient,
M_{cr}: Elastic buckling moment, it can be calculated from following equation.

$$M_{cr} = S_X\left(\left(\frac{1380A_F}{dL_b}\right)^2 + \left(\frac{20700}{(L_b/r_T)^2}\right)^2\right) \quad (5)$$

S_X : elastic section modulus about major axis, cm^3
A_F: area of compression flange, cm^2
d: height of section, cm
L_b: Unsupported length of purlin, cm
r_T :radius of gyration about minor axis of a section comprising the compression flange plus one sixth of web area, cm

5. Results and Discussion

The effect of corrugated steel sheeting on the moment resistance of Z-section purlins is considered. The ratio of improvement in moment capacity and failure mode of purlins is studied. Resistance of purlins without and with corrugated sheets was evaluated. Effect of changing sheeting height was also considered. The results are compared with the ECP [21] and AISI [22].

5.1. Effect of sheeting restrained at tension flange

From linear Eigen analysis, Figure 9 shows the elastic buckling modes of Z-purlins without sheeting for Z175*1.5 with span 2m and 8m. As can be seen from the figures, local buckling occurs for small spans (2m) for all Z-sections except for Z-sections (Z175*2.5, Z200*2.5 and Z265*2.5) are overall buckling. Also, overall buckling occurs for long spans (4m,6m,8m and10m) of all Z-sections except for Z-section Z265*1.5 of length 4m is local buckling.

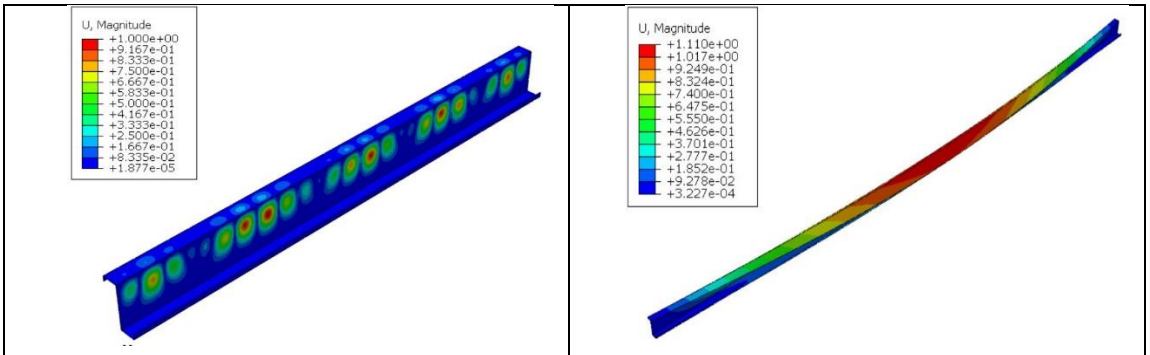

M_{cr}=10.85KN.m

a) Section Z175*1.5 with length 2m

M_{cr}= 0.529KN.m

b) Section Z175*1.5 with length 8m

Fig 9. linear analysis of purlin without sheeting

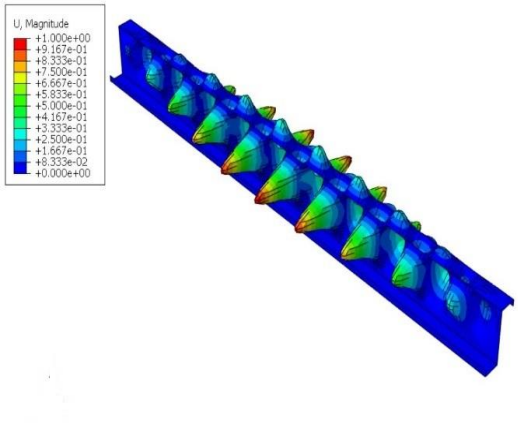

M_{cr}=10.88KN.m

a) Section Z175*1.5 with length 2 m

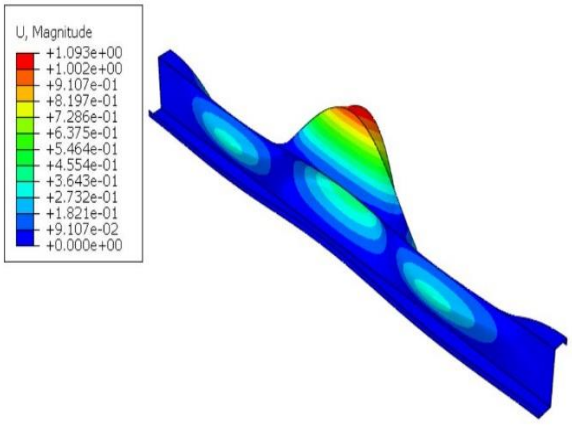

M_{cr}=19.62KN.m

b) Section Z175*2 with length 2 m

Fig 10. linear analysis of purlin with sheeting with length 2 m

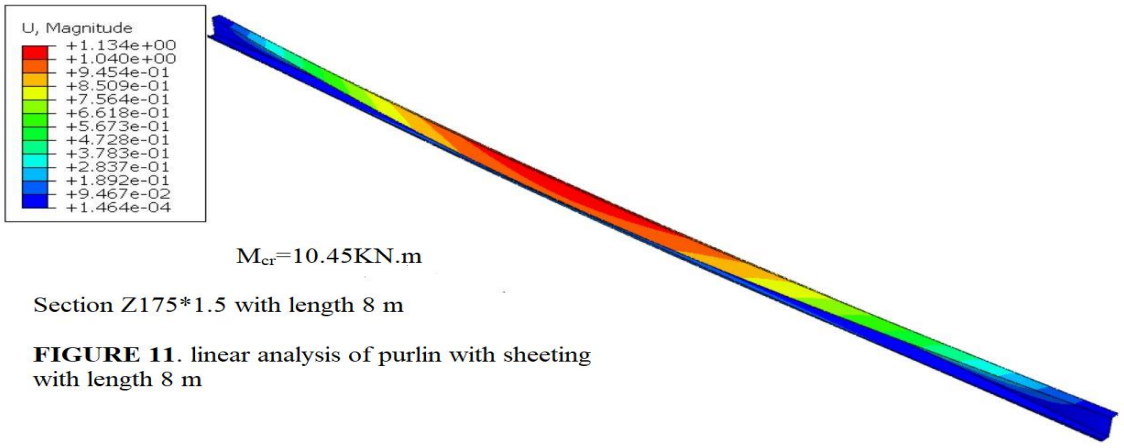

M_{cr}=10.45KN.m

Section Z175*1.5 with length 8 m

FIGURE 11. linear analysis of purlin with sheeting with length 8 m

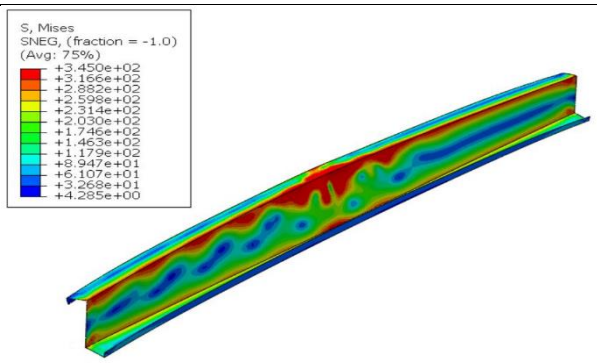

a) Whole Member

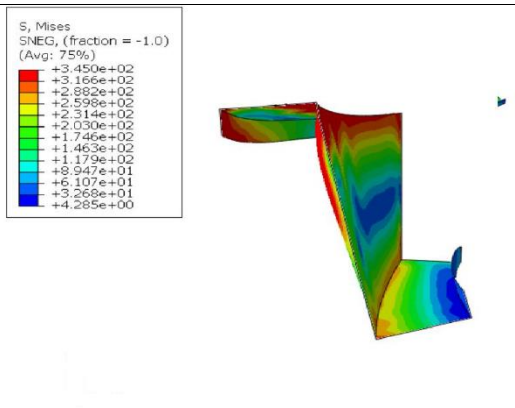

b) Section at mid span

Fig12. Failure mode of purlin without sheeting for section Z175 with thickness1.5mm, length 2m. (Mn=7.10KN.m)

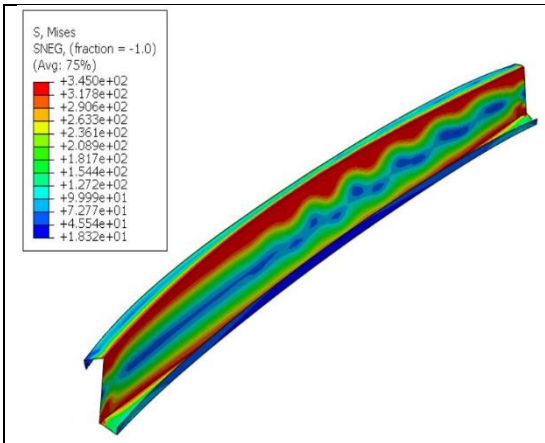

a) Whole Member

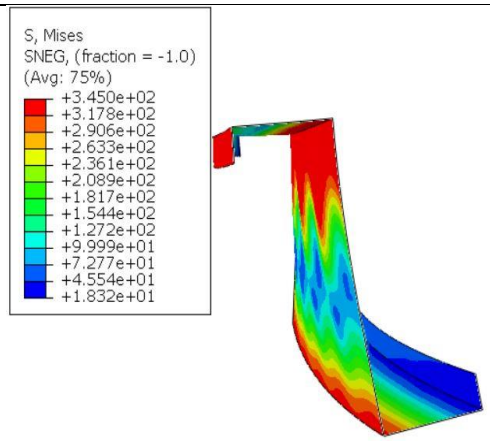

b) Section at mid span

Fig13. Failure mode of purlin without sheeting for section Z175 with thickness2mm, length 2m. (Mn=9.98KN.m)

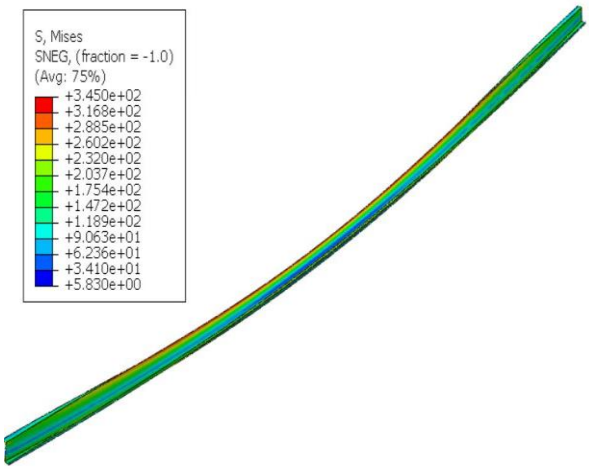

a) Whole Member

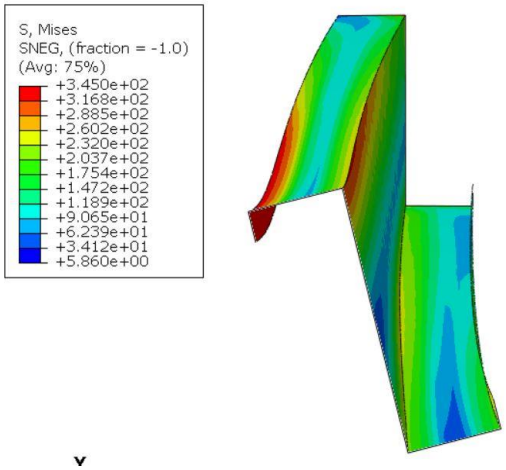

b) Section at midspan

Fig14. Failure mode of purlin without sheeting for section Z175 with thickness 1.5mm, length 8m (Mn=0.81KN.m)

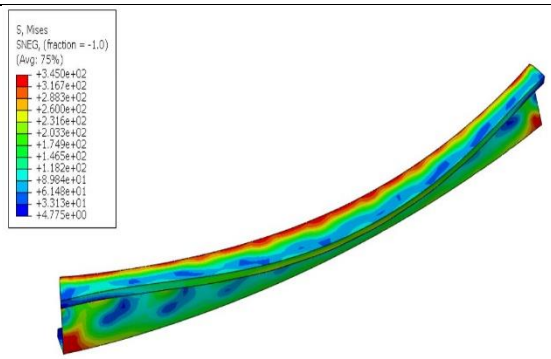

a)Whole Member

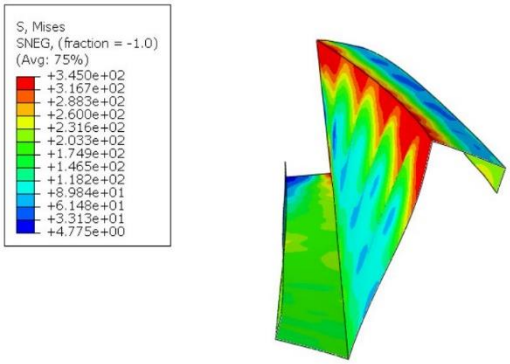

b)Section at mid span

Fig15. Failure mode of purlin with profile No.1 sheeting for section Z175 with thickness1.5,length 4m (Mn=5.47KN.m)

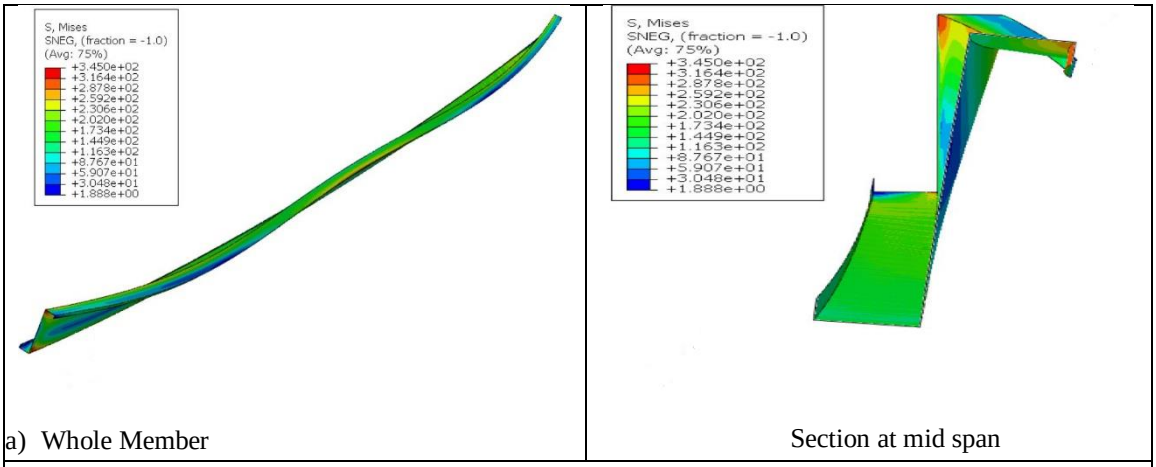

a) Whole Member Section at mid span

Fig16. Failure mode of purlin with profile No.1 sheeting for section Z175 with thickness1.5mm, length 8m (Mn=5.44KN.m)

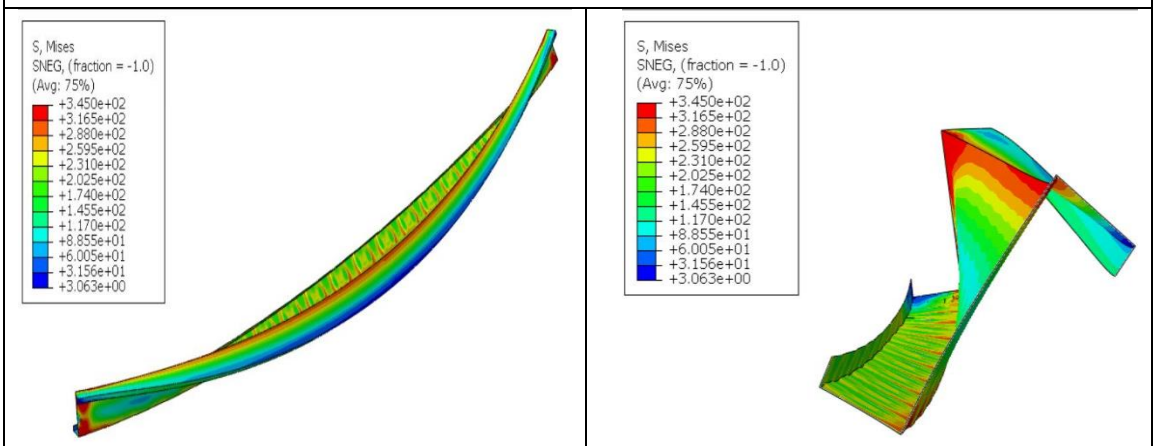

a) Whole member b)section at mid span

Fig17. Failure mode of purlin with profile No.2 sheeting for section Z175 with thickness1.5mm, length 4m (Mn=6.09KN.m)

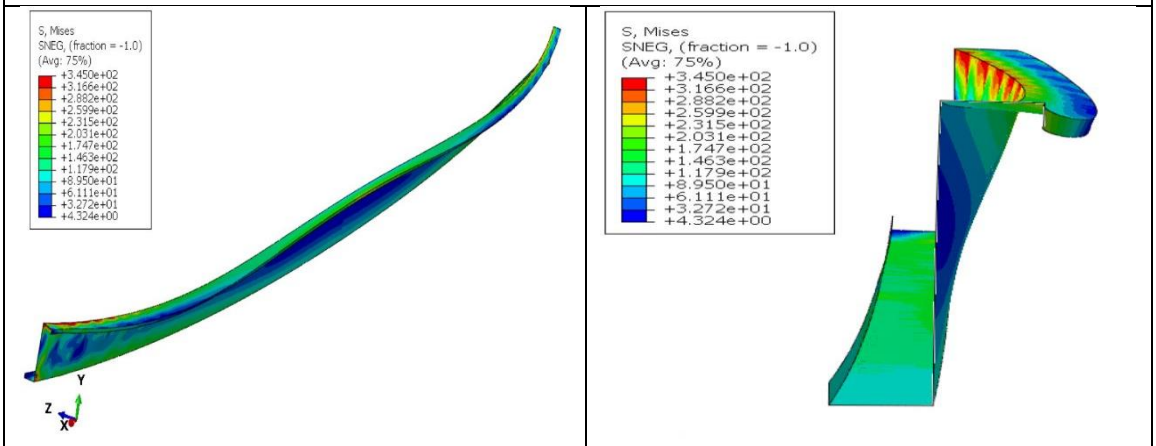

a) Whole member b)section at mid span

Fig18. Failure mode of purlin with profile No.2 sheeting for section Z175 with thickness1.5mm, length 8m (Mn=5.92KN.m)

For purlin with sheeting, the elastic buckling modes of Z-purlin for small span (2m) is local buckling for Z-section (Z175*1.5, Z200*2, Z200*2.5, Z265*1.5, Z265*2, Z265*2.5) while for others sections (Z175*2, Z175*2.5, Z200*2) buckling modes are distortional buckling as shown in Figure10. For long span, interaction between distortional and lateral torsional buckling occurs as shown in Figure 11.

For non-linear analysis, Figures 12 and 13 show non-linear analysis of Z-section without sheeting of length 2m. As shown in the figure, the failure modes of this section and all similar sections are distortional buckling except for sections (Z175*2, Z175*2.5, Z200*2, Z200*2.5) the failure modes are interaction between distortional and overall buckling. This is also noted for purlins with span 4 m. Figure 14 show the failure mode of long span 8m of Z-section without sheeting. As seen in the figure, the failure mode is overall buckling followed by yield stress of compression flange at web-flange junction and the flange-lip junction. This is also noted for purlins with spans (6 and 10m).

Figures15, 16, 17 and 18 show the failure modes of Z purlins with considering sheeting profile No.1 and profile No.2 connected to tension flange. As shown in the figures, the failure modes of all sections for all spans are interaction between distortional and overall buckling of all sections, accompanied by yield stress at web-flange junction. However, for long spans (8 and 10m) the failure modes do not show clear yield stress at web-flange junction for section at mid-section. Because the corrugated steel sheeting provides a full lateral brace along the length of the purlin and a partial rotation brace at tension flange, which improve the nominal flexural strength and alter the failure mode of purlin

Figures 19 and 20 depict the load-lateral displacement at web-flange junction of the free flange, at the mid-span for purlins with and without various profile of sheeting for section Z175*1.5. As shown in the figures, the nominal moment of section Z175*1.5 with length 4m is close with the nominal moment of the same specimen of length 8m. This may be attributed to the restraint provided by sheeting along the length of the specimen, so that the failure is caused by section capacity not member capacity. When moment is applied to the specimen, the lateral displacement rises until it reaches its maximum value, after that, the structure becomes less rigid until it fails. It was observed that for free flanges (compression flange) the horizontal lateral displacement of purlins without sheeting is greater than that of purlins with sheeting. The ultimate moment of a purlin with sheeting is greater than the ultimate moment of a purlin without sheeting due to action of sheeting, which offers some constraint that reduces the lateral movement of the free flange. Additionally, the curve of a purlin without sheeting is more ductile and exhibits less moment capacity than a purlin with sheeting. The moment resistance of Z-purlin with profile No.1 is smaller than moment resistance of Z-purlin with profile No.2. Additionally, a purlin with sheeting profile No.2 has a smaller lateral displacement than a purlin with profile No.1. This effect is due to the higher stiffness of profile sheeting No. 2 compered to stiffness of profile-sheeting No. 1. So that profile sheeting No. 2 produce greater rotational and lateral resists for attached purlin, consequently reduces lateral movement of free flange.

Figure 21 illustrates a comparison of the FEA results and codes results. Nine curves with various sections are taken into consideration. Figure 21 illustrates the relationship between M_n/M_y and the global slenderness ratio (λ_d). Where M_n is the nominal capacity moment of purlin, M_y is the initial yield moment of purlin. λ_d is defined as $\sqrt{\frac{M_y}{M_{cre}}}$, where M_{cre} is the critical elastic global buckling moment. M_{cre} is acquired from the CUFSM software [25]. Every curve starts at λ_d <0.94. For purlins without sheeting, the ratio M_n/M_Y decreases as the slenderness ratio increases. A reduction in the strength of these purlins may be attributed to the overall lateral torsional buckling occurrence, which governs the failure of purlins without sheeting.

The figure reveals that the effect of sheeting on the tension flange of a Z-purlin results in a great improvement in the purlin's flexural capacity. For λ_d<0.94, the nominal moment for purlin with profile No.1 sheeting is changed with slenderness ratio. Therefore, the beam slenderness ratio has an impact on the R factor. As for the short spans with low slenderness ratio, the effect of sheeting on moment capacity of purlin is insignificant as the failure mode is section capacity.

For longer spans where λd>0.94, the nominal moment of purlin with profile No.1 sheeting (M_1) is higher than the nominal capacity moment of purlin without sheeting (M_n), because the corrugated steel sheeting acts as a restraint along the length of purlin. The average ratio of M_1/M_n for sections Z175, Z200, and Z265 are 5.490, 4.293 and 4.192, respectively.

The effect of the web-depth-to-thickness ratio on the average Mn/My ratio of Z-purlin is considered. For purlin without sheeting, the h/t ratios of Z-purlin (Z175) are 116.67, 87.5 and 70, with average ratio (Mn/My) ratios of 0.271, 0.288 and 0.301, respectively. The ratios (h/t) of Z-section (Z200) are 133.33, 100, and 80, and the average ratios (Mn/My) are 0.267, 0.301 and 0.303, respectively. The ratios (h/t) for Z-section (Z265) are 176.67, 132.5, and 106 and the average ratios (Mn/My) are to be 0.254, 0.277 and 0.301 respectively.

For purlin linked with sheeting, the (h/t) ratios for Z-section (Z175) are 116.67, 87.5 and 70 average, with (Mn/My) ratios of 0.271, 0.288, and 0.301. The (h/t) ratios for Z-section (Z200) are 133.33, 100 and 80, with average (Mn/My) ratios of 0.497, 0.597, and 0.599. The h/t ratios for Z-section (Z265) are 176.67, 132.5 and 106, with average Mn/My ratios of 0.455, 0.529, and 0.575.

The comparisons between the nominal moments calculated using various codes and the nominal moments obtained from the finite element model are shown in Figure 21. The nominal moment of the finite element of a purlin linked with sheeting for ƛd<0.94 is greater than the nominal moment of AISI-codes because section capacity is the failure mode. Therefore, the R factor that is recommended by AISI affected by the slenderness ratio.

The nominal strength capacity of purlin attached to sheeting for ƛd>0.94 obtained from finite element is in good agreement with the nominal moment evaluated by AISI for all Z-sections except for sections (Z200*2 and Z265*2). For these sections finite element results are slightly greater than flexural moment of AISI by about 9% and11% respectively. For purlins without sheeting, the results of the finite element model are in good agreement with the AISI code for sections Z175, Z200, and Z265 with average percentage of increase of about 2.16%, 0.573% and 1.19%.

For ECP, the nominal moment of purlin obtain from finite element model is greater than the nominal moment evaluated by ECP code, with an average increasing percentage for sections Z175, Z200, and Z265 of about 41.4%, 44.1 and 44.7 in case of ƛd<0.94. While for ƛd>0.94, the average percentage increase to about 53%, 54% and 68%.

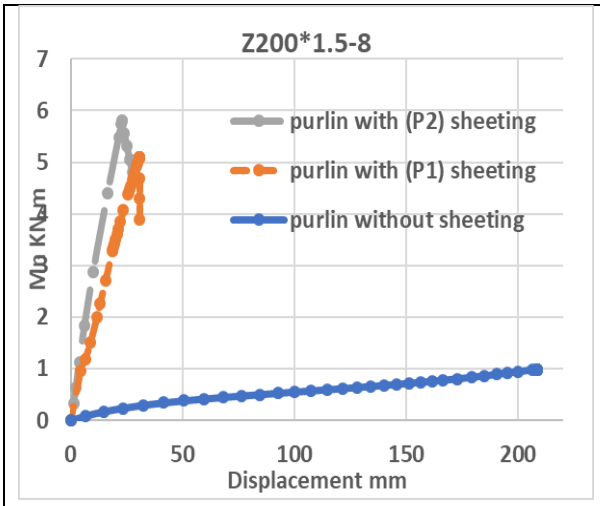

a) For span (8m)

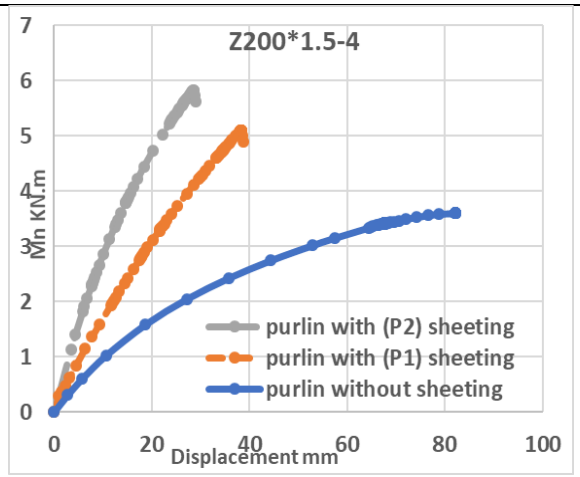

b)For span (4m)

Fig19. Load displacement curve for purlins Z200 with thickness 1.5mm, 4m and 8m spans

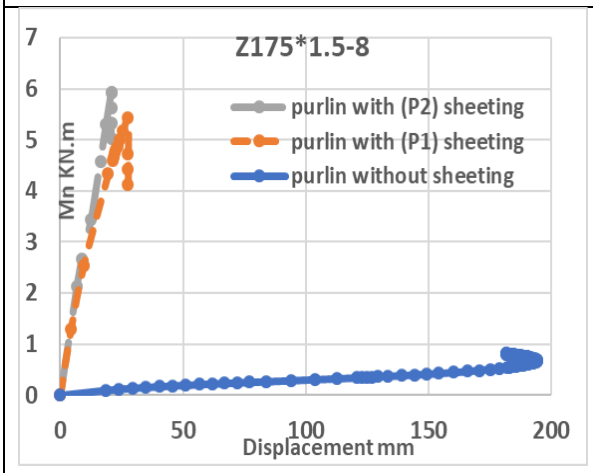

a) For span 8m

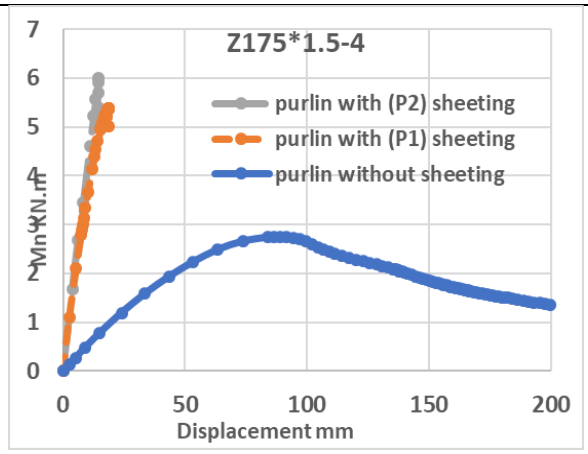

b)For span 4m

Fig20. Load displacement curve for purlins Z175 with thickness1.5mm, 4m and 8m spans

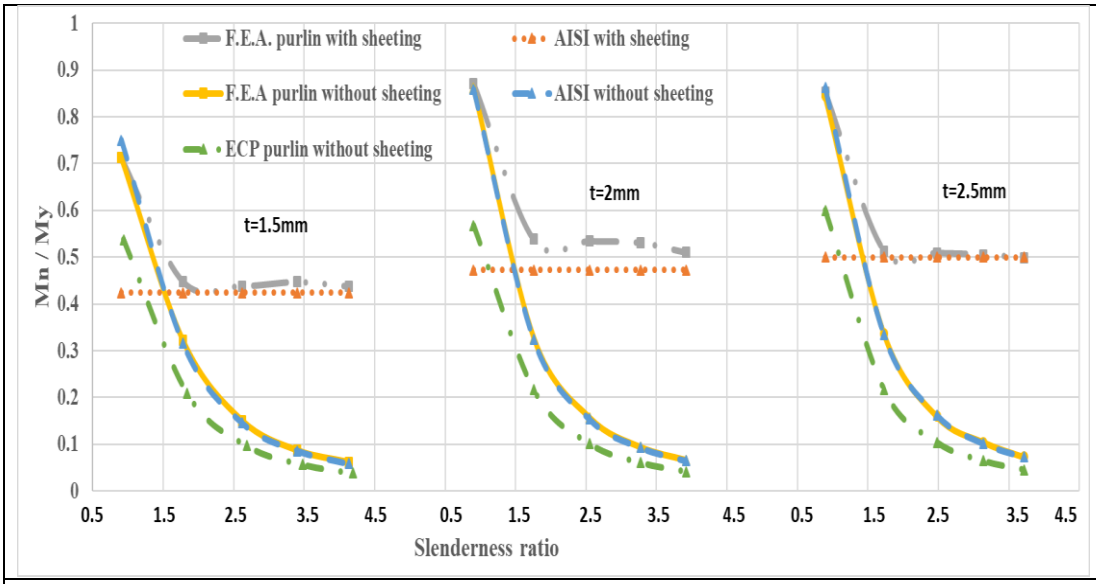

a)Section Z175 without and with profile sheeting No.1 for different thickness

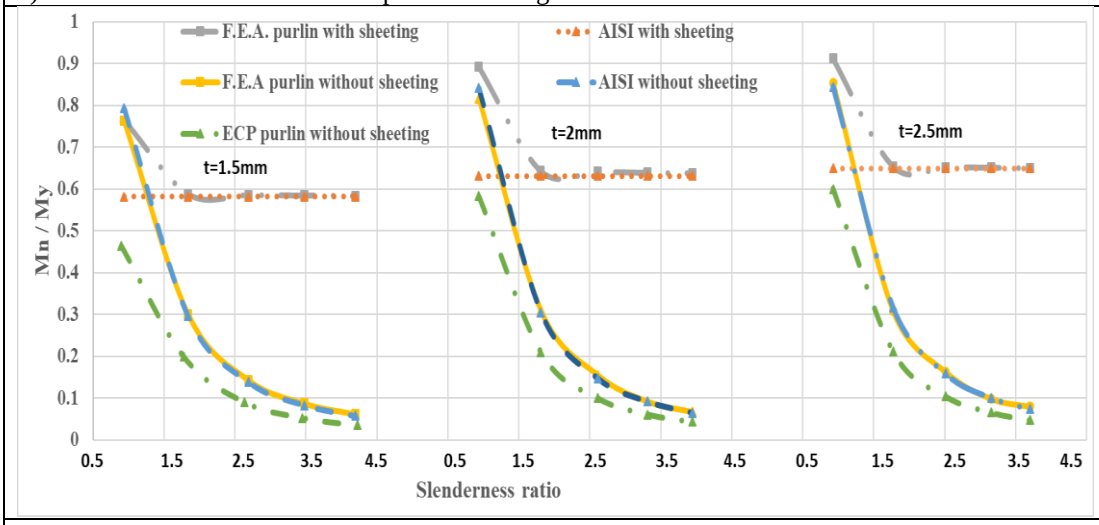

b)Section Z200 without and with profile sheeting No.1 for different thickness

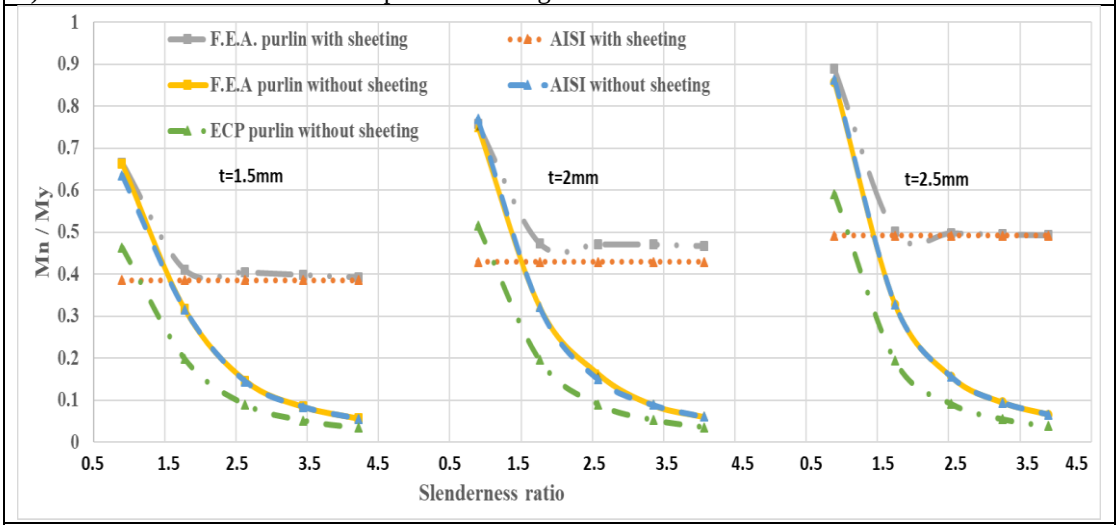

c)Section Z265 without and with profile sheeting No.1 for different thickness

Fig 21. Variation of M_n/M_y to Slenderness ratio (λ_d)

5.2. Effect of changing the profile type of sheeting

The results of the investigation of the nominal strength of purlins with various profile sheets obtained from Finite element analysis are shown in Figure 22. The specimens that are used, as shown in the figure, have lengths ranging from 4m to 10m, disregarding the impact of short lengths (2m). Purlins connected to profile sheeting No. 2 have nominal moments for all of their sections that are greater than those connected to profile sheeting No. 1, because the profile's wave height increases from 25mm to 50mm. So that profile sheeting No. 2 is stiffer. For section Z175, the average percentage increase in moment capacity from using profile No. 2 to profile No. 1 is 7.45%. Additionally, for section Z200, there is an average percentage increase of 9.94% in the moment capacity of the purlin from using profile sheeting No. 2 to profile sheeting No. 1. For section Z265, the nominal moment of the purlins increased by 11.15% from using profile sheeting No. 2 to using profile sheeting No. 1.

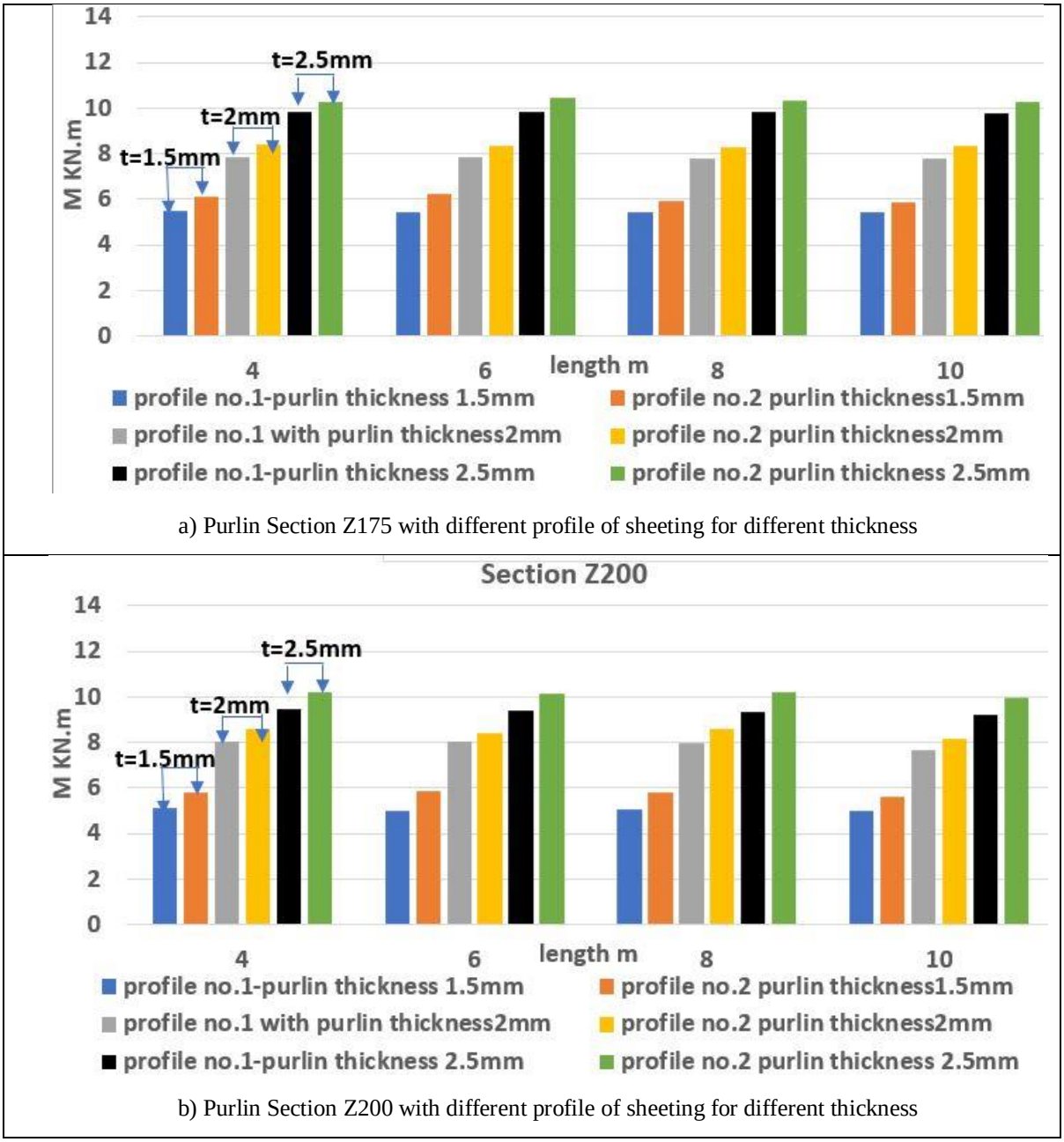

a) Purlin Section Z175 with different profile of sheeting for different thickness

b) Purlin Section Z200 with different profile of sheeting for different thickness

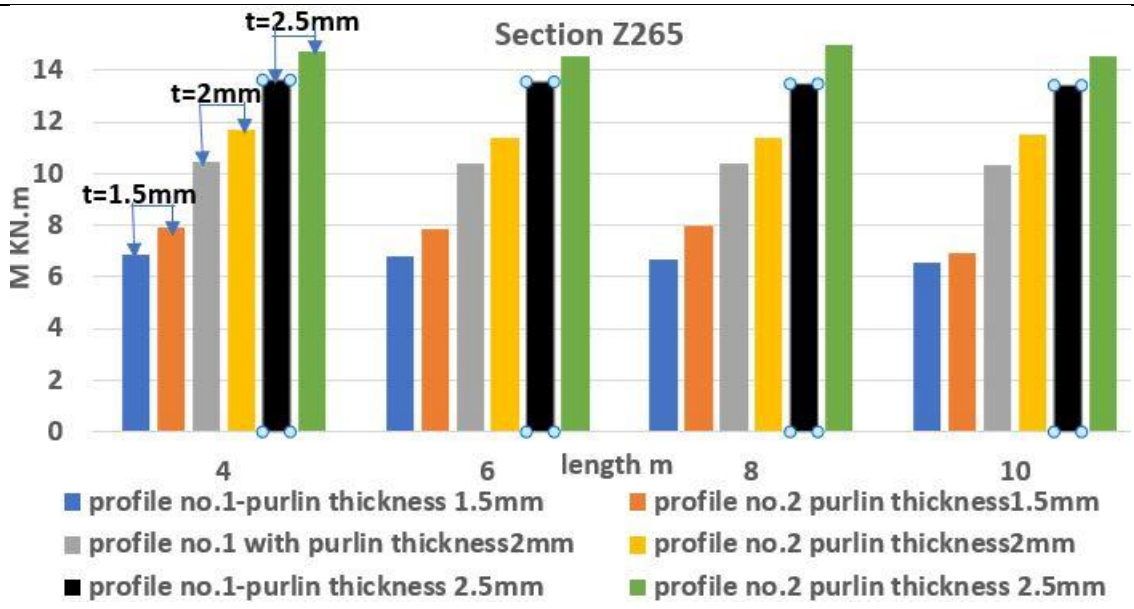

c) Purlin Section Z265 with different profile of sheeting for different thickness

Fig 22. The effect of profile No.1 and profile No.2 on the moment capacity of purlins

6. Summary and Conclusions

A numerical parametric study has been conducted to evaluate the ultimate flexural strength of Z-purlins under two equal end moments. In the modeling process, the influence of corrugated steel sheeting restraining the tension flange on the moment capacity of Z-sections is considered. Results of the parametric study showed that:

1- Considering the lateral restraint effect of the tension flange by the corrugated sheets, the failure modes of long-span Z-purlins change from overall lateral torsional buckling to mainly sectional buckling modes; either local or distortional depending on the beam span.

2- The nominal moment capacity of long span Z-purlins increases significantly by considering the lateral restraint of the tension flange. This enhancement of the nominal flexural capacity on average is up to 200% for all sections.

3- The height of the corrugated sheet affects the nominal flexural capacity of the Z-purlins with the tension flange laterally restrained. The average nominal flexural capacity increases by about 10% with increasing height of the corrugated sheets. The percentage increase varies from 4% to 15% for all sections.

4- The nominal flexural capacity of the Z-purlins with a laterally restrained tension flange provided by North American Specifications, AISI-S100, is comparable with the FEA results for purlins with slenderness ratios, $\lambda_d > 0.94$. However, for purlins with $\lambda_d < 0.94$, the predicted nominal moments of AISI are lower than those of FEA.

5- Finite element results show that the reduction factor "R" of Z-purlins with tension flange laterally braced is affected by beam slenderness ratio as well as the corrugated sheet profile. This conclusion has to be considered in AISI provisions to get more accurate estimation of nominal flexural resistance.

References

[1] Ye, J., Hajirasouliha, I., Becque, J., & Pilakoutas, K. (2016). Development of more efficient cold-formed steel channel sections in bending. *Thin-walled structures*, *101*, 1-13.

[2] Guimarães, V. M., Gilbert, B. P., Talebian, N., & Wang, B. (2021). Shape optimisation of singly-symmetric cold-formed steel purlins. *Thin-Walled Structures*, *161*, 107402.

[3] Dundu, M. (2011). Design approach of cold-formed steel portal frames. *International Journal of Steel Structures*, *11*, 259-273.

[4] Zhang, L., & Tong, G. S. (2016). Lateral buckling of simply supported C-and Z-section purlins with top flange horizontally restrained. *Thin-Walled Structures*, *99*, 155-167.

[5] Ye, Z. M., Kettle, R., & Li, L. Y. (2004). Analysis of cold-formed zed-purlins partially restrained by steel sheeting. *Computers & Structures*, *82*(9-10), 731-739.

[6] Li, L. Y. (2004). Lateral–torsional buckling of cold-formed zed-purlins partial-laterally restrained by metal sheeting. *Thin-walled structures*, *42*(7), 995-1011.

[7] Luan, W., & Li, Y. Q. (2019). Experimental investigation on wind uplift capacity of single span Z-purlins supporting standing seam roof systems. *Thin-walled structures*, *144*, 106324.

[8] Chu, X. T., Rickard, J., & Li, L. Y. (2005). Influence of lateral restraint on lateral-torsional buckling of cold-formed steel purlins. *Thin-Walled Structures*, *43*(5), 800-810.

[9] Gao, T., & Moen, C. D. (2012). Direct Strength Design of Metal Building Wall and Roof Systems-Through-fastened Simple Span Girts and Purlins with Laterally Unbraced Compression Flanges. Proceedings of the 21st International Specialty Conference on Cold-Formed Steel Structures, University of Missouri-Rolla, St Louis, Missouri, USA.

[10] Balázs, I., Melcher, J., & Belica, A. (2016). Experimental investigation of torsional restraint provided to thin-walled purlins by sandwich panels under uplift load. *Procedia Engineering*, *161*, 818-824.

[11] Li, Y. & Ma, R. & Song, Y. & Pan, S... (2013). Experimental study on shear behavior of screw connections for cold-formed thin-walled steel structures. 41. 11-19.

[12] Ren, C., Li, L. Y., & Yang, J. (2012). Bending analysis of partially restrained channel-section purlins subjected to up-lift loadings. *Journal of Constructional Steel Research*, *72*, 254-260.

[13] Ren, C. (2013). *Structural behavior of cold-formed steel purlin-sheeting systems under uplift loading* (Doctoral dissertation, University of Birmingham).

[14] Zhu, J., Chen, J. K., & Ren, C. (2014). Numerical study on the moment capacity of zed-section purlins under uplift loading. *Structural Engineering and Mechanics*, *49*(2), 147-161.

[15] Zhang, Y., Xue, J., Song, X., & Zhang, Q. (2018). Numerical parametric analysis of the ultimate loading-capacity of channel purlins with screw-fastened sheeting. *International Journal of Steel Structures*, *18*, 1801-1817.

[16] Huang, R., & Luan, W. (2020, June). COMPARISON of Chinese and Foreign Specifications on Bending Behavior of Z-Purlins under Wind Uplift Load. In *IOP Conference Series: Earth and Environmental Science* (Vol. 525, No. 1, p. 012169). IOP Publishing.

[17] Yu, C., & Yan, W. (2011). Effective Width Method for determining distortional buckling strength of cold-formed steel flexural C and Z sections. *Thin-walled structures*, *49*(2), 233-238.

[18] Wibbenmeyer, K. D. (2010). Determining the R values for 12 inch deep Z-purlins and girts with through-fastened panels under suction loading.

[19] Almatrafi, M., Theofanous, M., Dirar, S., & Gkantou, M. (2021). Structural response of cold-formed lipped Z purlins–Part 1: Experimental investigation. *Thin-Walled Structures*, *161*, 107452.

[20] Almatrafi, M., Theofanous, M., Dirar, S., & Bock, M. (2021). Structural response of cold-formed lipped Z purlins–Part 2 numerical modelling and optimisation of lip size. *Thin-Walled Structures*, *161*, 107453.

[21] Egyptian Code of Practice for Steel Construction (Load and Resistance Factor Design -LRFD). Permanent Committee for the Code of Practice for Steel Construction and Bridges. First Edition 2008. Arab Republic of Egypt Ministry Of Housing, Utilities And Urban Development

[22] AISI S100-16(R2020) w/S3-22: North American Specification for the Design of Cold-Formed Steel Structural Members, 2016 Edition (Reaffirmed 2020) With Supplement 3, 2022 Edition.

[23] Hibbitt, K. (2012). Inc. ABAQUS. ABAQUS/Standard User's Manual Volumes I-III and ABAQUS CAE Manual.

[24] Albion Sections. Z-purlin, cladding rail and Eaves beams technical manual. (2019). http://albionsections.co.uk/doc/52.pdf

[25] Schafer, BW, Adany, S. (2006). Buckling analysis of cold-formed steel members using CUFSM: conventional and constrained finite strip methods. In: Proceedings of the 18th international specialty. onference on cold-formed steel structures. Orlando, FL, United states: University of Missouri-Rolla.